

# **Micromechanical Effects of Chemical Weathering on Carrara Marble**

A. Wubalem, C. Caselle, A.M. Ferrero, G. Umili

*University of Torino, Torino, Italy  
[azemerawwubalem.azeze@unito.it](mailto:azemerawwubalem.azeze@unito.it)*

M.R. Migliazza, F. Vagnon

*Politecnico di Torino, Torino, Italy*

## **Abstract**

Chemical-induced alteration of geo-materials often linked to climatic factors such as acid rain, can lead to a worsening of the mechanical characteristics. Thus, understanding how Carrara marble responds to acid rain is vital for effective engineering design and historical heritage preservation.

This study investigates the mechanical response and strain evolution of Carrara marble under varying durations of simulated sulphuric acid rain exposures (0, 3, 7, and 28 days) using uniaxial compressive tests and digital image correlation (DIC). Thirteen prismatic marble samples were prepared and grouped into four sets. The first set is used as an untreated base and other sets are used for 3, 7, and 28 days of sulphuric acid immersion (pH=5). Mechanical testing under uniaxial compression eventually quantified the mechanical worsening induced by the weathering. A series of video films were recorded using two optical cameras. Then DIC analysis was performed for selected images of strain moment from elastic, plastic, peak, and post-peak regions of the stress-strain curves.

The result shows acid bath exposure causes a general reduction in the mechanical strength and elastic modulus. This indicates that Carrara marble is susceptible to acidic environments which could affect its long-term durability in construction and cultural heritage preservation.

This paper represents the preliminary phase of an ongoing research project focused on the effects of deterioration related to freeze-thaw cycling and/or chemically aggressive environments through mechanical tests and microscale investigation techniques.

## **Keywords**

Chemical Weathering, Strain Evolution, Uniaxial Compressive Strength, Digital Image Correlation

## **1. Introduction**

Carrara marble has been a famous building stone in construction and sculptures since ancient civilizations because of its uniform white color, high density, strength, and fine-medium-grained calcite crystals (Calvo and Ragueiro 2010; Vagnon et al. 2021). However, climate-related environmental stressors, particularly chemical weathering, cause substantial threats to its strength and durability. This weathering process commonly occurs in areas exposed to chemically polluted environments (Wu et al. 2023). Acid rain, which contains sulfuric acid, causes a significant risk as it can dissolve the carbonate minerals, accelerating the degradation of the marble. This can result in deterioration of structures made of marble such as buildings, monuments, and statues. Therefore, evaluating the Carrara marble's response to acid rain is crucial for effective engineering design and the preservation of historical buildings. While the effects of thermal weathering on various rocks have been extensively studied (Fan et al. 2020; Han et al. 2017; Hou et al. 2022; Park et al. 2020; Sarfarazi et al. 2024; Zhang et al. 2023), the impact of chemical weathering, particularly sulphuric acid rain, on the micro-mechanical degradation of Carrara marble remains insufficiently investigated.

This study aims to investigate the effects of simulated sulphuric acid rain on the micro-mechanical properties of Carrara marble. Marble samples were immersed in a sulphuric acid solution at pH 5 for 3, 7, and 28 days. Changes in strength and deformation behaviour were assessed through uniaxial compressive strength tests, linear variable differential transformer (LVDT) measurements, and Digital Image Correlation (DIC) analysis. The findings can enhance our understanding of how Carrara marble responds to acid environments and contribute to the development of effective preservation strategies for historical buildings.

## **2. Materials and methods**

Carrara marble is a metamorphic rock formed under the polyphasic tectonic-metamorphic deformation of the northern Apennine orogenic belt (Coli & Criscuolo 2021). It exhibits variability in color, ranging from white and statuary to veined and grey.

The tested material is white fine-medium-grained Carrara marble, mainly composed of calcite grains, with minor dolomite and trace amounts of terrigenous minerals. A total of 13 prismatic samples 60x30x30 mm, were prepared from six 60x60x60mm cubic blocks (see Fig. 1 a). These samples were grouped into four groups. The first group was used as untreated bases, while the second, third, and fourth groups were subjected to acid rain chemical weathering simulation for 3, 7, and 28 days, respectively.

This study simulated sulfuric acid rain-induced chemical weathering for 3, 7, and 28 days of exposure. The samples were washed with clean deionized water. Then, they were immersed in a  $5 \times 10^{-6}$  mol/l acid solution of pH 5 inside a rectangular bath (see Fig. 1b). The acid bath was then placed inside a protected environment covered by glasses (see Fig. 1c). After 3 days of acid bath exposure, the samples belonging to the second set were removed from the solution. They were carefully rinsed with clean water and dried in an oven at 105 °C. The third and fourth sets of specimens were kept in the solution for 7 and 28 days, respectively, and were then rinsed and dried in the same manner.

The uniaxial compressive strength (UCS), stress-strain curve, and tangential Young's modulus were determined for untreated and treated samples. These tests were performed using the Matest compressive servo plus testing machine in the Applied Geology Laboratory of the Department of Earth Sciences at the University of Turin. The machine has a maximum load capacity of 300 kN and the tests were performed under displacement control. Axial displacement was measured throughout the test using an axial LVDT. Axial stress was applied at a constant rate of 0.036- 0.037 mm/min (corresponding to a strain rate of  $10^{-5}$ /s) with a pre-loading of 2 kN.

DIC analysis (Blaber et al., 2015; Caselle et al., 2019; Ferrero & Migliazza, 2009; Stirling et al., 2013; Zhang et al. 2020), was performed after UCS tests. The lateral surfaces of the samples were cleaned, and a rectangle line was drawn on the sample surface using a permanent black marker to help the software track deformations. For each sample, two videos were recorded on two adjacent lateral faces before and during loading until sample failed, using two optical cameras (see Fig. 1e) with the assistance of Basler video recording open-source software installed on laptops (see Fig. 1d). Each video frame was extracted using the open-source free video-to-JPG converter software. For each

video, 9-18 frames were then selected corresponding to specific moments of the stress-strain curve (e.g., elastic phase, strain onset, peak, post-peak) and subsequently analyzed through DIC analysis principles using the Ncorr software (Blaber et al., 2015) coupled with MATLAB R2024b. Strain maps derived from digital image correlation analysis are presented according to Ncorr sign convention.

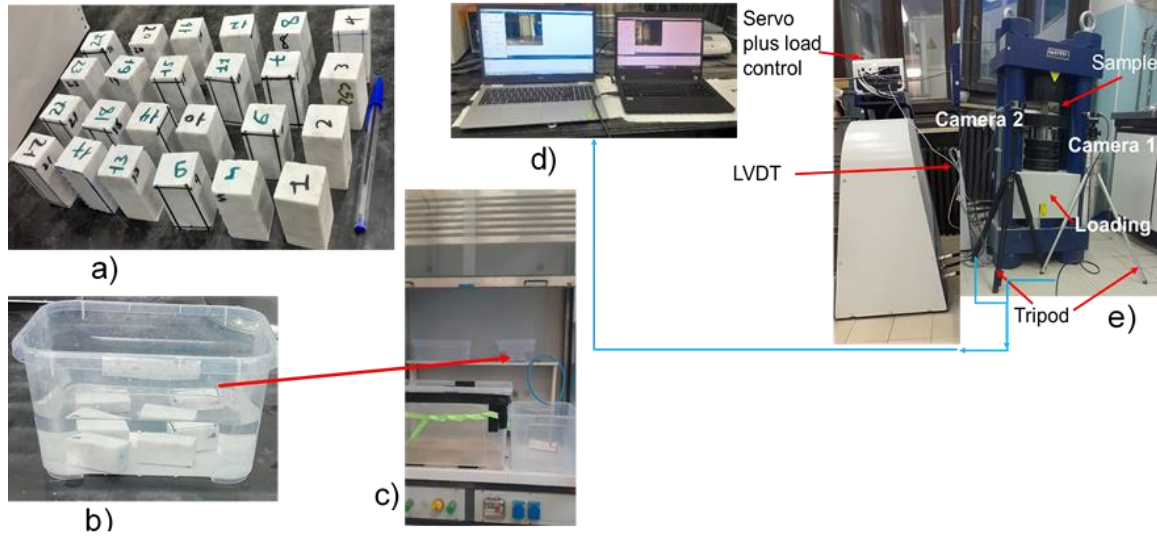


Fig. 1a) Samples used in this study and b) after immersion in the acid solution under the lab glass-covered hood (c), d) Laptop configuration, and e) uniaxial compressive strength apparatus and cameras set up

### 3. Result and discussion

#### 3.1 Uniaxial compressive strength and elastic modulus

Table 1 presents UCS and tangential Young's modulus ( $E_t$ ) values for untreated and acid-treated samples. The results reveal that despite considerable variability of results, untreated samples showed the highest mean uniaxial compressive strength in the datasets (93.72 MPa), with a standard deviation of 18.51 MPa. Untreated samples' highest and lowest UCS values are 115.9 MPa and 74.1 MPa, respectively. The mean tangential Young's modulus ( $E_t$ ) is approximately 21.53 GPa, with a standard deviation of 8.62 GPa, reflecting variability in stiffness.

After 3 and 7 days of acid bath exposure, UCS, and tangent Young's modulus decline moderately (Table 1). This could be due to micro-mechanical degradation induced by acid treatment. After 28 days of the acid bath, the mean UCS and  $E_t$  significantly decreased to 30.68% and 44.733%, respectively, compared to untreated samples. This indicates that the sample has experienced micro-failures or internal damage during acid bath exposure further confirmed by multiple stress drops before failure (Fig. 3 d).

Table 1 Uniaxial compressive strength and tangent Young's modulus of untreated and treated samples

Acid bath days	Samples	UCS [MPa]	Mean [MPa]	std [MPa]	$E_t$ [GPa]	Mean [GPa]	std [GPa]
0	M21	83.8	93.72	18.51	-	21.53	8.62
	M22	74.1			12.4		
	M23	115.9			29.6		
	M24	101.1			22.6		
3	M1	71.9	89.11	14.89	10.9	19.37	7.37
	M2	97.3			24.4		
	M4	98.1			22.8		
7	M5	98.8	86.34	11.62	27.8	19.29	7.05
	M6	91.7			22.4		
	M7	71.8			12.8		
	M8	83.1			14.2		
28	M10	47.4	64.96	24.86	11.6	11.90	0.47
	M11	82.5			12.2		

Fig. 2 reports the number of acid bath days against the mean UCS (see Fig. 2 a) and the mean tangent Young modulus (see Fig. 2 b). The result indicates that UCS decreases as the days of acid bath

exposure increase (see Fig. 2 a), identifying a linear relationship. Similarly, tangent Young's modulus also showed a linear decline with acid bath exposure (see Fig. 2 b). The reduction in mechanical strength, and loss of material stiffness after treatment shows the progressive degradation of marble samples. Thus, Carrara marble seems vulnerable to degradation under acidic environments, which can aggravate structural vulnerabilities, causing wear, deformation, and failure.

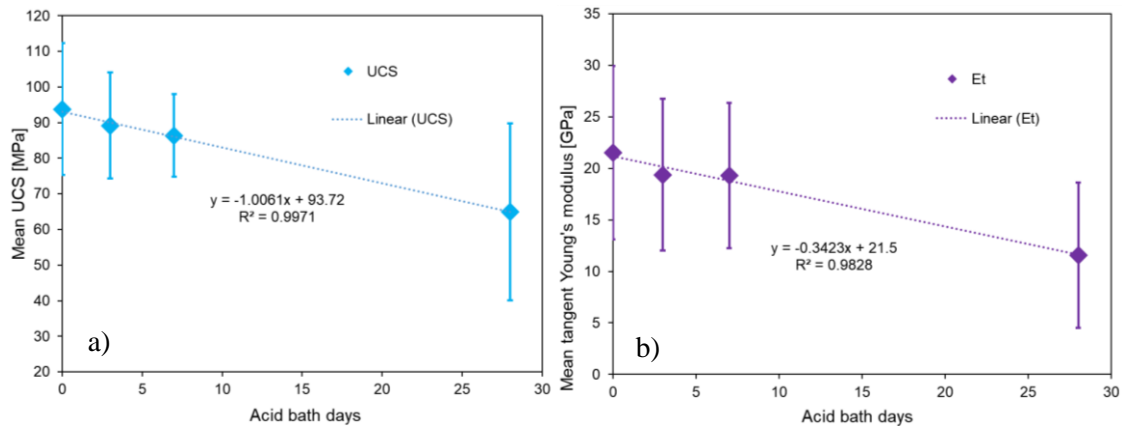


Fig. 2 Relationship between a) mean uniaxial compressive strength and acid bath exposure days and b) mean tangent Young's modulus and acid bath exposure days

### 3.2 Stress-strain curve

Stress-strain curves present how acid exposure affects the behaviour of marble under uniaxial compression (see Fig. 3). Initially, the stress-strain relationship is non-linear, possibly due to the closure of existing micro-fractures then changes to linear as the loading increases. Untreated samples show relatively higher peak stress, and steepest elastic slope, indicating greater compressive strength. In contrast, for samples exposed to an acid bath, peak stress, and elastic slope relatively decrease with increased acid bath exposure, suggesting the weakening of materials.

The strain behavior of 0, 3, and 7 days of acid-treated samples generally show less strain at peak stress (see Fig. 3 a, b, and c). Samples after 28 days of acid bath display higher strain before failure and lower in peak stress. The strain at peak stress for most samples occurs between 0.0048 and 0.009. The untreated samples reach their peak stress around 0.005-0.008 strain, indicating failure at low deformation. The treated samples particularly after 28 days of acid bath reached their peak around 0.0095 strain, indicating slightly higher strain values than other samples, which failed at high deformation. Although strains show variability across samples, generally it increases as acid bath exposure increases. The post-peak behavior is characterized by numerous resistance drops (see Fig. 4, 5 and 6), suggesting a stick-slip behavior, consistent with what has been observed at the laboratory scale by several authors in different lithology's (e.g., Caselle et al. 2020).

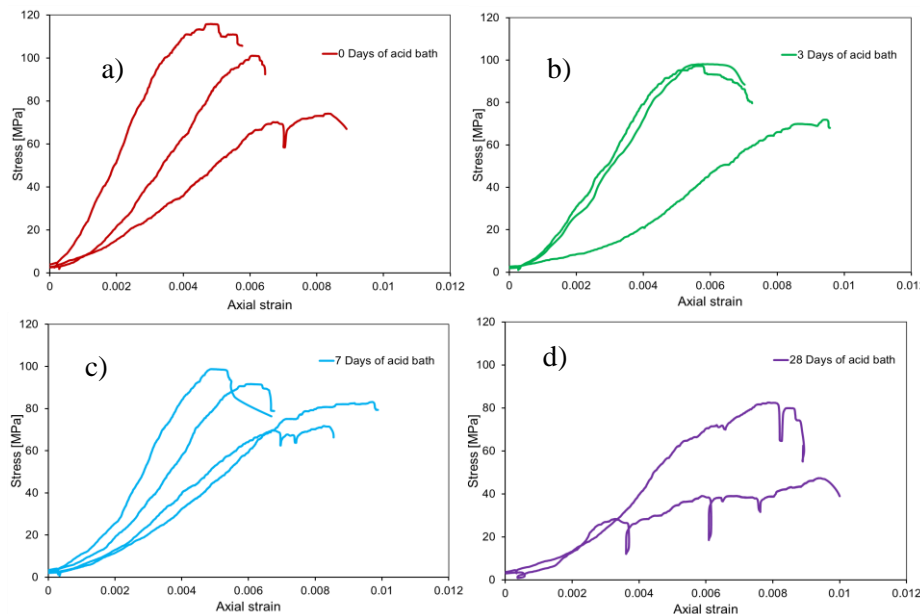


Fig. 3 Stress-strain curves a) 0 days of acid bath b) 3 days of acid bath c) 7 days of acid bath and d) 28 days of acid bath

### 3.3 DIC analysis and fracture evolution

#### 3.3.1 Untreated samples (0 Days of acid bath)

Fig.4 shows strain maps (iii) in the horizontal axis at different stages of loading corresponding to points labeled on stress-strain curves a-n (see Fig.4 i) representing various phases of deformation for an untreated sample. As can be seen from Fig.4iii, the results show a relatively uniform distribution of strains (the blue color, corresponds to low strain) with some localizations that become more evident and coherent after reaching the peak. Around point d-e, strains are propagated and relatively well distributed. Strains at points e-f, light blue, green, yellow, and red zones are more localized, indicating the beginning of damage. They (g-n) become increasingly localized into intensive isolated red zones, typically, at point n, strains are fully concentrated with macroscopic crack development and eventual failure. These fracture progression zones reflect the propagation and widening of fractures. The combined result of the stress-strain curve and DIC maps reveal the mechanical behavior of the sample under uniaxial compressive loading. The relatively uniform strain in the early stages indicates a relatively homogenous response. However, the post-peak fracture development phase does not occur homogeneously but is characterized by “jumps”, which are also clearly evident in the stress-strain curve (see Fig.4i), suggesting a stick-slip type of behavior.

In general terms, the DIC results highlight brittle fracture mechanisms for the untreated samples, with very clear strain localizations in the maps (see Fig.4 iii). The sample failure occurs following tensile strain concentrations localized in a few sample areas. The photographic image of the post-failure sample (see Fig.4 ii) shows the presence of two very well-defined coalescent failure planes consistent with the brittle nature identified by the stress-strain curve and with the location of the high-strain concentration zones identified by the DIC maps (see Fig.4 iii).

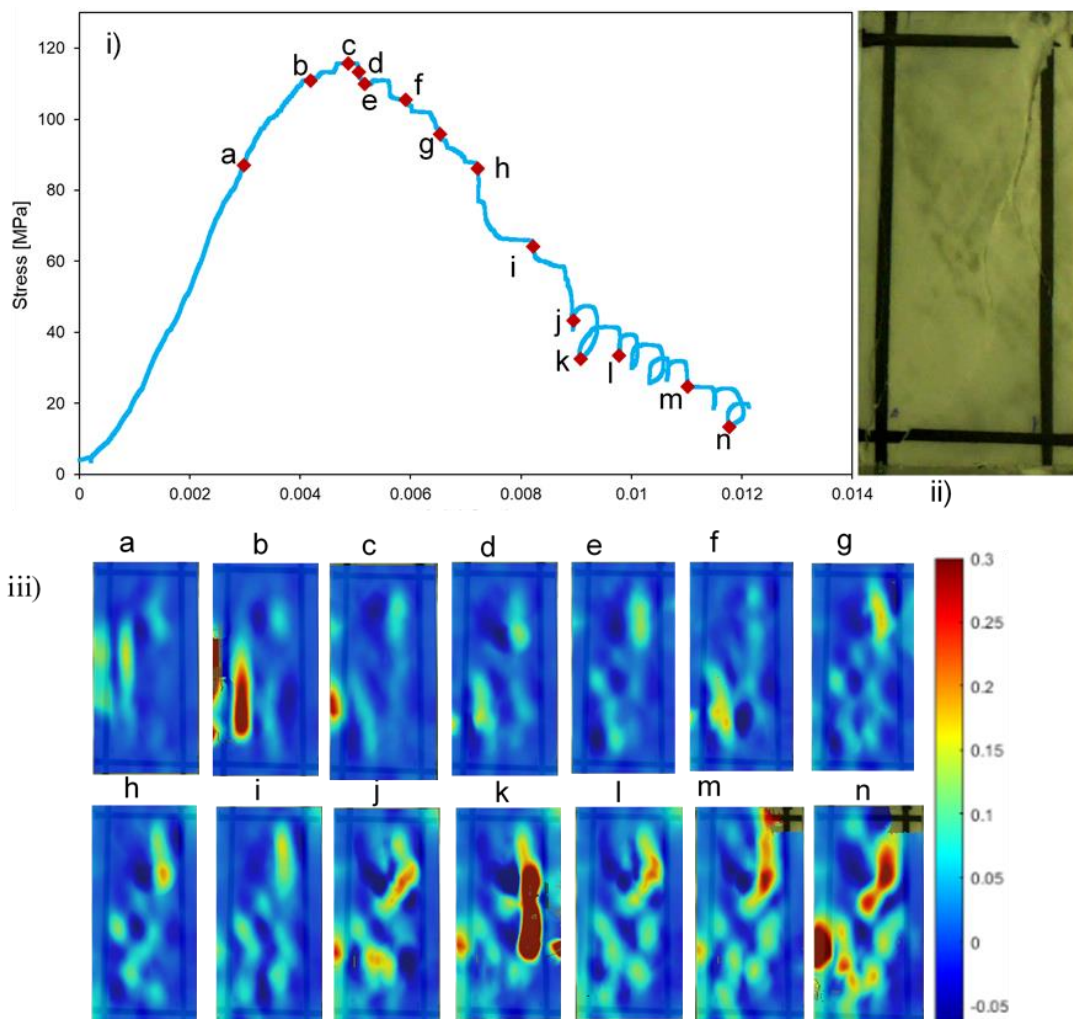


Fig. 4 i) Stress-strain curves ii) sample after the peak , iii) digital image correlation strain maps in horizontal axis ( $E_{xx}$ ) of untreated samples

### 3.3.2 3 Days of acid bath

Lateral strains are less concentrated in the early stages, and high strain zones in red are more distributed across the sample (see Fig. 5 iii). The crack propagation and failure appear more gradual, with multiple smaller strain concentrated zones formed before the crack coalesces. The strain maps revealed that strain evolutions are localized along different stages. In the initial stages (stage 1) to 28% of stress (see Fig. 5 i), the overall strain distribution remains relatively uniform except for a few localized strains (point a). At this stage, no cracks have been initiated. When the sample is loaded with 64% stress (stage 2), the rock is in the elastic deformation stage (points b and c), and a certain increase in the recorded strain concentrations is observed (light blue, green, and yellow colors). In stage 3 (points d and e), the onset of the deformation and then the peak strength are reached. At this stage, the maps show an increase in the length of the detected strain concentrations, suggesting that the microfractures, which were already starting to form during the elastic phase, can organize and coalesce. In the post-peak phase (stage 4), the fractures grow in an unstable manner, with increasingly extended strain concentrations and higher strain values (points f, g, h, and i). In the last phase (stage 5) the resistance decreases rapidly and drastically due to the fractures that are now interconnected with each other, leading to the complete failure of the sample. Furthermore, the post-failure sample (see Fig. 5 ii) shows two major fracture surfaces which appear to be consistent with the location of the major strain concentrations identified by the DIC maps.

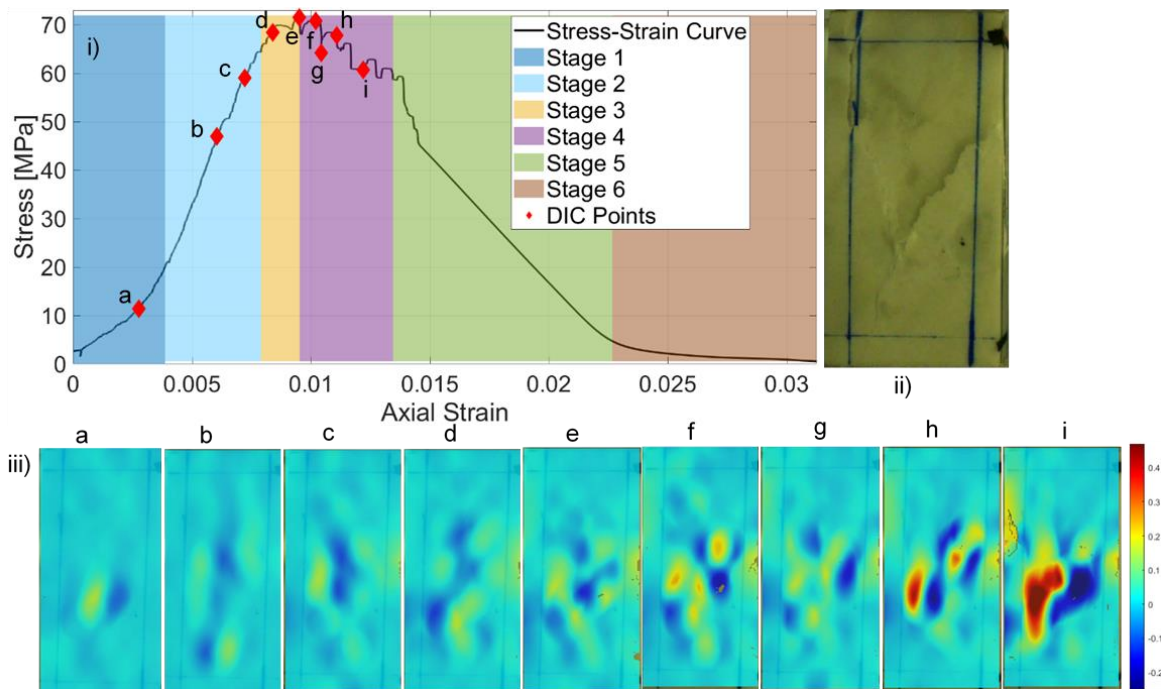


Fig. 5 i) Stress-strain curves, ii) sample after the peak, iii) digital image correlation strain maps in the horizontal axis ( $E_{xx}$ ) after 3 days of the acid bath

### 3.3.3 7 Days of acid bath

As seen in Fig. 6 iii, strain maps demonstrate how the samples deform laterally ( $E_{xx}$ ) along the horizontal axis perpendicular to the loading direction. In early stages (a-d), lateral strains are very few, but near the peak (e-g) a few strain concentrations (light blue) begin, but lateral expansion is still very low. From points (h-k), a linear strain is more localized in different bands, indicating macroscopic fractures. At points (m-s), significant lateral strains are observed, indicating crack widening and material separation. The higher strain values in red confirm lateral expansion, particularly near the failure zones. This showed the DIC strain maps clearly show an elastic-plastic and post-peak transition, with crack initiation, propagation, and coalescence. The actual image on the top right (see Fig. 6 ii) and linear strain localization (red) confirm that DIC captures the sample deformation accurately. Compared to the previously described samples, a greater gradualness in the development of the fracture is observed.

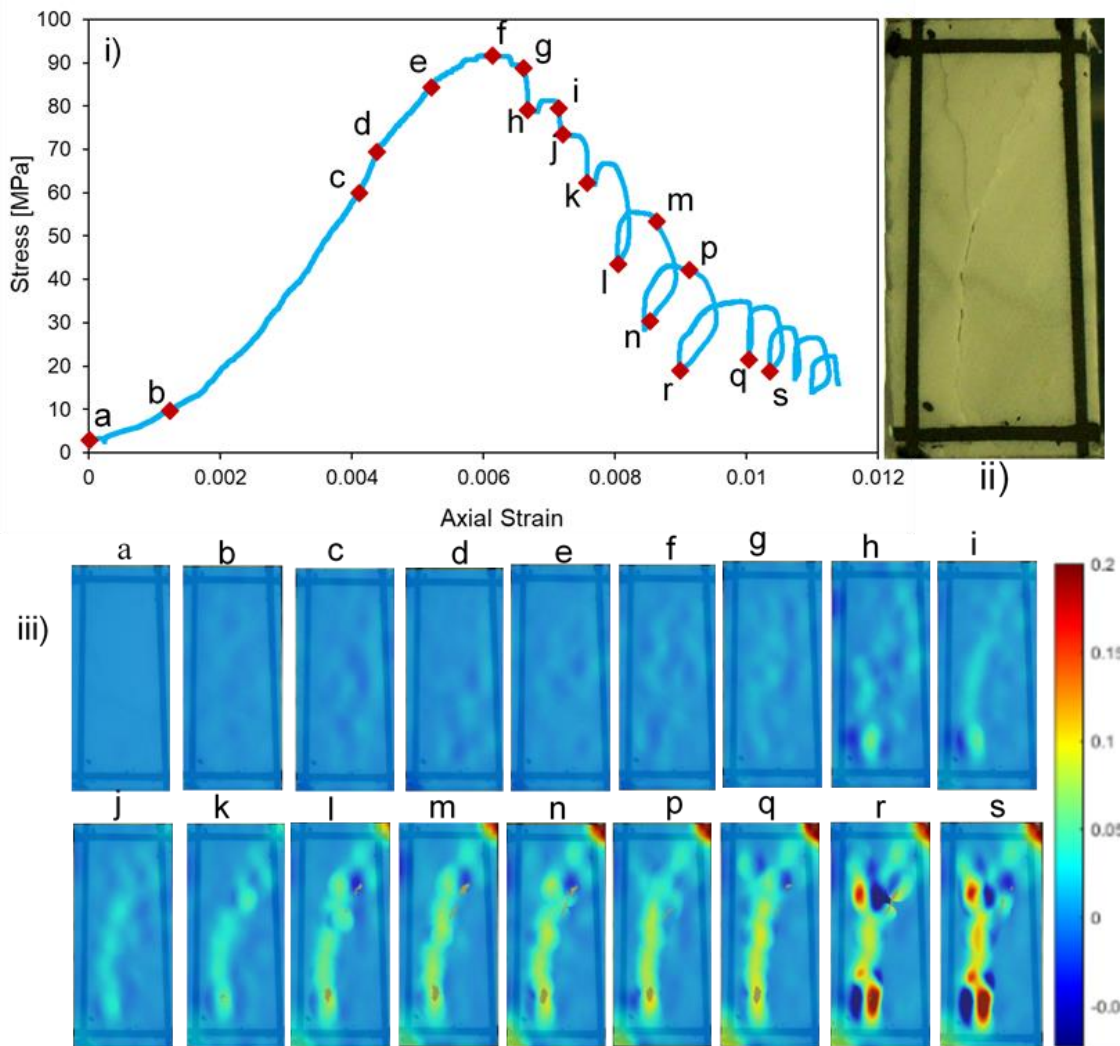


Fig. 6 i) Stress-strain curves, ii) sample after the peak, iii) digital image correlation strain maps in the horizontal axis ( $E_{xx}$ ) after 7 days of the acid bath

#### 4. Conclusion

This study investigated the effects of sulphuric acid exposure on the mechanical behavior of Carrara marble. The changes in uniaxial compressive strength, elastic modulus, and strain evolution during loading were experimentally studied. The uniaxial compressive strength and elastic modulus generally decrease as the number of days of acid bath exposure increases. Similarly, the failure mechanism is significantly affected by the acid treatment. These results suggested that the mechanical properties of Carrara marble deteriorate due to the acid treatment. Untreated samples show high peak stress, and relatively steep elastic slope compared to treated samples. In post-peak, both untreated and treated samples show stick-slip behaviour, which could be due to fracture propagation, coalescence, and stress redistribution. The stress-strain curve, in conjunction with DIC strain maps, highlights the stages of deformation, which start with crack initiation, propagation, and coalescence, eventually leading to the failure of the marble samples under uniaxial compression. The early stages (compaction and elastic) are characterized by uniform strain distribution and minimal damage, while the post-peak stages are predominantly marked by significant strain localization and extensive fracturing. This indicates that DIC is a powerful tool for understanding strain evolution and provides valuable insight into tracking the failure mechanism of rocks under compression. Based on DIC analysis and experiment, fracture evolution increases as the sample approaches failure, with samples experiencing shear, and tensile failures.

The reduction in both UCS and Et after prolonged acid bath exposure underscores the importance of considering and assessing the chemical resistance of rock in engineering design and preservation of historical buildings. This study mainly focused on the effects of acid exposure on the mechanical

strength and deformation behaviour of marble rock. In future work, the microscopic changes of marble after the acid exposures and freeze-thaw cycling will be assessed in detail using scanning electron microscopy, digital image correlation, and micro-computed tomography.

## References

- Blaber J, Adair B & Antoniou A (2015) Ncorr: Open-Source 2D Digital Image Correlation Matlab Software. *Experimental Mechanics* 55(6): 1105-1122. <https://doi.org/10.1007/s11340-015-0009-1>.
- Calvo JP & Regueiro M (2010) Carbonate rocks in the Mediterranean region from classical to innovative uses of building stone. *Geological Society Special Publication* 331:27-35. <https://doi.org/10.1144/SP331.3>.
- Caselle C, Bonetto S & Costanzo D (2020) Crack coalescence and strain accommodation in gypsum rock. *Frattura Ed Integrità Strutturale* 14(52):247-255. <https://doi.org/10.3221/IGF-ESIS.52.19>.
- Caselle C, Umili G, Bonetto S & Ferrero AM (2019) Application of DIC analysis method to the study of failure initiation in gypsum rocks. *Geotechnique Letters* 9(1):35-45. <https://doi.org/10.1680/jgele.18.00156>.
- Coli M & Criscuolo A (2021) The Carrara Marble: Geology, geomechanics and quarrying 833(1). <https://doi.org/10.1088/1755-1315/833/1/012120>.
- Fan L, Xu C & Wu Z (2020) Effects of cyclic freezing and thawing on the mechanical behavior of dried and saturated sandstone. *Bulletin of Engineering Geology and the Environment* 79(2):755-765. <https://doi.org/10.1007/s10064-019-01586-z>.
- Ferrero AM & Migliazza MR (2009) Theoretical and numerical study on uniaxial compressive behaviour of marl. *Mechanics of Materials* 41(5):561-572. <https://doi.org/10.1016/j.mechmat.2009.01.011>.
- Han T, Shi J, Chen Y & Cao X (2017) Physical and mechanical properties of marble under the combined effects of chemical solutions and freeze-thaw cycles. *Geotechnical Testing Journal* 40(6):1057-1070. <https://doi.org/10.1520/GTJ20160225>.
- Hou C, Jin X, He J & Li H (2022) Experimental studies on the pore structure and mechanical properties of anhydrite rock under freeze-thaw cycles. *Journal of Rock Mechanics and Geotechnical Engineering* 14(3):781-797. <https://doi.org/10.1016/j.jrmge.2021.10.005>.
- Park K, Kim K, Lee K & Kim D (2020) Analysis of effects of rock physical properties changes from freeze-thaw weathering in Ny-Ålesund region: Part 1-experimental study. *Applied Sciences (Switzerland)* 10(5):1707. <https://doi.org/10.3390/app10051707>.
- Sarfarazi V, Torabi-Kaveh M & Moayedi Far A (2024) Effects of weathering depth and thickness on rock failure: Experimental approach and particle flow code simulation. *Journal of Rock Mechanics and Geotechnical Engineering* 16(11) :4638-4653. <https://doi.org/10.1016/j.jrmge.2023.11.046>.
- Stirling RA, Simpson DJ & Davie CT (2013) The application of digital image correlation to Brazilian testing of sandstone. *International Journal of Rock Mechanics and Mining Sciences* 60:1-11. <https://doi.org/10.1016/j.ijrmms.2012.12.026>.
- Vagnon F Costanzo D, Ferrero AM, Migliazza MR, Pastero L & Umili G (2021) Simulation of temperature and chemical weathering effect on marble rocks 833(1). *Mechanics and Rock Engineering, from Theory to Practice*, IOP Conf. Series: Earth and Environmental Science, Turin, Italy, 20-25 September 2021, 833(1). <https://doi.org/10.1088/1755-1315/833/1/012068>.
- Wu J, Lu Y, Wang K, Cai Y & Xiao C (2023) Combined effects of freeze-thaw cycles and chemical corrosion on triaxial mechanical properties of sandstone. *Geomechanics and Geophysics for Geo-Energy and Geo-Resources* 9(1). <https://doi.org/10.1007/s40948-023-00588-2>.
- Zhang R, Yang Y, Ma D & Ping, Q (2023) Experimental study on effect of freeze-thaw cycles on dynamic mode-I fracture properties and microscopic damage evolution of sandstone. *Engineering Fracture Mechanics* 279. <https://doi.org/10.1016/j.engfracmech.2023.109043>.